



Theoretical and experimental investigation of on-chip mid-infrared chalcogenide waveguide CH₄ sensor based on wavelength modulation spectroscopy

Mingquan Pi^a, Yijun Huang^a, Huan Zhao^a, Zihang Peng^a, Jiaming Lang^a, Jialin Ji^a, Ling Teng^b, Fang Song^{a,*}, Lei Liang^c, Yu Zhang^a, Chuantao Zheng^{a,*}, Yiding Wang^a, Frank K. Tittel^d

^a State Key Laboratory of Integrated Optoelectronics, College of Electronic Science and Engineering, Jilin University, 2699 Qianjin Street, Changchun 130012, China

^b School of Mathematics and Statistics, Changchun University of Science and Technology, Changchun 130022, China

^c State Key Laboratory of Luminescence and Applications, Changchun Institute of Optics Fine Mechanics and Physics, Chinese Academy of Sciences, Changchun 130033, China

^d Department of Electrical and Computer Engineering, Rice University, 6100 Main Street, Houston, TX 77005, USA

ARTICLE INFO

Keywords:

Waveguide gas sensor
Wavelength modulation spectroscopy
Chalcogenide waveguide
CH₄ sensor
On-chip sensor

ABSTRACT

Compared with direct absorption spectroscopy (DAS), wavelength modulation spectroscopy (WMS) with good ability of suppressing noise is rarely used in waveguide sensor. The influence of waveguide parameters on WMS sensing performance is required to clarify in both theory and experiment. Three mid-infrared waveguide methane (CH₄) sensors (trapezoid, rectangular, suspended) were proposed and optimized for WMS simulation. Theoretical formulation and the experimentally derived sensing noise were used to numerically evaluate the key figure of merit more accurately. Simulation results were presented to show the influence of waveguide parameters on sensing performance. Two chalcogenide on magnesium fluoride (ChG-on-MgF₂) trapezoid waveguide CH₄ sensors were fabricated using lift-off method, and CH₄ measurement was carried out using WMS. The waveguide loss was measured to be 1.52 dB/cm, leading to an optimal sensor length of 2.7 cm. The limit of detection (LoD) of CH₄ for the 1cm- and 2cm-long waveguide sensors are 0.68% and 0.17% with an averaging time of 0.2 s. The experimentally achieved second harmonic (2f) signal amplitude and LoD show good agreement with the theoretical results, verifying the feasibility of the design and analysis model of the WMS-based waveguide sensor. Due to the use of WMS and a reduction of waveguide loss from 3.6 to 1.52 dB/cm, the LoD of the 2cm-long ChG-on-MgF₂ sensor is 24 times lower than our previously reported 2cm-long ChG-on-SiO₂ sensor based on DAS. This work provides a systematic guidance for the design of waveguide gas sensor based on WMS and contributes to improving the sensitivity of on-chip gas sensing.

1. Introduction

Direct absorption spectroscopy (DAS) and wavelength modulation spectroscopy (WMS) are two commonly-used techniques for gas detection [1–5]. Compared with DAS, WMS processes sensing signal at a high frequency region to suppress noise and reveals better performance [6]. For a gas sensing system with bulk discrete units (e.g., gas cell, lens), the free-space light passing through a gas cell without the target analyte can be considered lossless and the contribution of long optical path (generally m to km scale) to enhance light-gas interaction is obvious.

However, this kind of sensing system is large in size and is easily affected by environmental vibration and consumes high power. Optical waveguide sensor integrated with a laser and a detector on a single-chip with small size can solve these problems, but the waveguide intrinsic loss α_{int} (mainly includes material absorption loss, scattering loss and bending loss), small sensing waveguide length L (generally mm to cm scale) and small external confinement factor γ (generally < 1) decrease absorption signal and signal-to-noise ratio (SNR). The factor γ indicates the interaction effect between light and gas molecular, where $\gamma = 1$ for free-space light absorption. A suspended waveguide with $\gamma = 107\%$ was proposed

* Corresponding authors.

E-mail addresses: songfang369@163.com (F. Song), zhengchuantao@jlu.edu.cn (C. Zheng).

<https://doi.org/10.1016/j.snb.2022.131782>

Received 27 December 2021; Received in revised form 15 February 2022; Accepted 23 March 2022

Available online 26 March 2022

0925-4005/© 2022 Elsevier B.V. All rights reserved.

for near-infrared (NIR) acetylene (C_2H_2) sensing based on DAS, but the non-negligible α_{int} made the limit of detection (LoD) larger than the free-space light sensing with the same optical path length [7].

Generally, the three parameters α_{int} , γ and L influence the performance of an on-chip sensor together. The main purpose for optimizing such a small-size sensor is decreasing LoD, which determines its application prospect. Five key issues to improve the performance of the on-chip gas sensor are as follows. (1) Selecting suitable core layer and cladding layer materials to decrease the material absorption loss at the operating wavelength. (2) Selecting and optimizing the waveguide structure to increase γ . (3) Considering the feasibility and cost of the fabrication process. (4) Selecting an appropriate L according to α_{int} to improve SNR. (5) Selecting appropriate spectroscopy sensing technique.

Design and simulation of a waveguide gas sensor are important for field applications. The performance of a waveguide gas sensor based on DAS was theoretically studied considering only the noise of the detector [8–18]. However, the LoD is affected by not only the noise from the detector but also the interference from some environmental factors, e.g. vibration. Instead of DAS, our group proposed a mid-infrared (MIR) chalcogenide (ChG) on magnesium fluoride (MgF_2) waveguide carbon dioxide (CO_2) sensor at ~ 4319 nm based on WMS for the first time [19]. Compared with DAS, the LoD was reduced by > 8 times by virtue of WMS. Under the same LoD requirement, the use of WMS is beneficial to the miniaturization of an on-chip waveguide sensor. However, detailed theoretical analysis of waveguide parameters on sensing performance has not been studied yet, and gas measurement is still needed to verify the analysis theory and simulation model for the design of a waveguide gas sensor based on WMS.

In this work, three typical mid-infrared waveguide methane (CH_4) sensors (trapezoid, rectangular, suspended) were proposed, and theoretical analysis, waveguide fabrication and gas measurement were conducted on two ChG-on- MgF_2 waveguide sensors. The novel aspects of this work include: (1) Theoretical formulation and simulation model of ChG waveguide gas sensor were proposed based on WMS. (2) The performances of three typical waveguides (trapezoid, rectangular, suspended) sensors were simulated by using the optimized waveguide parameters as well as some experimental parameters for high accuracy. (3)

Two optimized ChG-on- MgF_2 waveguides were fabricated for CH_4 measurement. (4) The LoD of the fabricated meander ChG-on- MgF_2 waveguide is 24 times lower than the ChG-on- SiO_2 sensor with the same length based on DAS. (5) The experimentally achieved relation between the amplitude of the second harmonic signal and waveguide length shows good agreement with the theoretical result.

2. Optical waveguide sensing theory and formulation

The sensing schematic diagram of a waveguide sensor based on WMS is shown in Fig. 1. For WMS operation, a high-frequency sinewave signal ($u_{sin}(t) = A_{sin}\sin(\omega_{sin}t)$) is added to a low-frequency triangular-wave scan signal $u_{tri}(t)$ to drive the laser. A_{sin} and ω_{sin} are the amplitude and angular frequency of $u_{sin}(t)$, respectively. The scan signal $u_{tri}(t)$ with an amplitude of A_{tri} ($0 \leq t \leq T_{tri}$) is expressed as [6].

$$u_{tri}(t) = \begin{cases} -A_{tri}/2 + (2A_{tri}/T_{tri})t, & 0 \leq t \leq T_{tri}/2 \\ 3A_{tri}/2 - (2A_{tri}/T_{tri})t, & T_{tri}/2 \leq t \leq T_{tri} \end{cases} \quad (1)$$

The drive signal $u_{WMS}(t)$ can be expressed as

$$u_{WMS}(t) = u_{tri}(t) + u_{sin}(t) \quad (2)$$

The signal $u_{WMS}(t)$ applied on the ICL results in a current signal $i(t)$ (in mA), which changes both the emitting wavenumber (ν , in cm^{-1}) and output power (P_0 , in mW). For the used ICL with a central wavelength of 3291 nm, the relation curves of ν and P_0 versus i at $16^\circ C$ are shown in Fig. 1(b) and the linear fitting equations are

$$\nu(t) = -0.15934i(t) + 3046.8152 \quad (3)$$

$$P_0(t) = 0.14445i(t) - 2.6969 \quad (4)$$

The absorption sensing theory of a waveguide CH_4 sensor obeys Lambert-Beer law [13,14], expressed as

$$P = P_0 \exp(-\gamma\alpha_{gas}CL - \alpha_{int}L) \quad (5)$$

where C is the CH_4 concentration; P is the waveguide output light power; α_{gas} is the CH_4 absorption coefficient, which can be obtained from the high-resolution transmittance (HITRAN) molecular spectroscopy

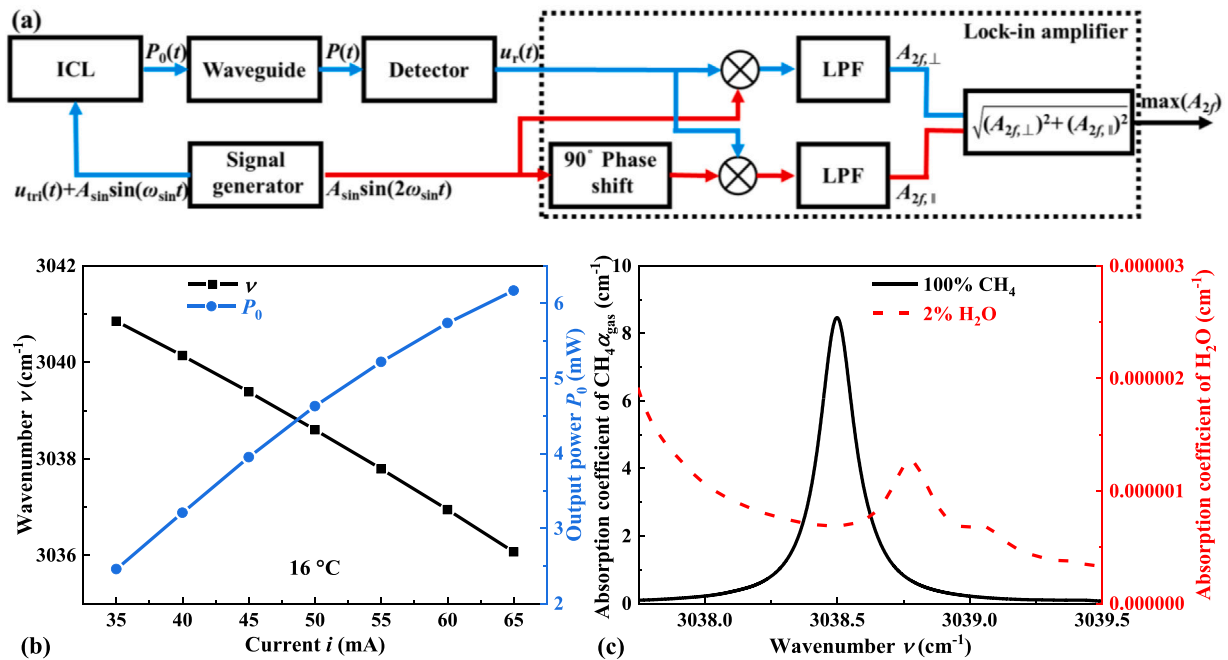


Fig. 1. (a) Schematic diagram of a waveguide sensor based on WMS. (b) Curves of ν and P_0 of the used ICL versus i at an operating temperature of $16^\circ C$. (c) The absorption coefficient α_{gas} of pure CH_4 and 2% H_2O versus wavenumber ν , where the ambient temperature is $27^\circ C$, the atmospheric pressure is 1 atm and the interaction length $L = 1$ cm.

database [21]. The α_{gas} of pure CH₄ and 2% H₂O versus ν is shown in Fig. 1(c) at an ambient temperature of 27 °C, an atmospheric pressure of 1 atm and an optical absorption length of $L = 1$ cm. The absorption coefficient of H₂O is 6 orders smaller of magnitude than CH₄, and the effect of H₂O can be neglectable. The external confinement factor γ can be expressed as [20].

$$\gamma = \frac{n_g \iint_{\text{gas}} \varepsilon(x, y) |E(x, y)|^2 dx dy}{n_{\text{gas}} \iint_{\text{total}} \varepsilon(x, y) |E(x, y)|^2 dx dy} \quad (6)$$

where E and ε are the electric field and permittivity of the waveguide cross-section in the z direction, respectively. n_g and n_{gas} are group index and the refractive index of the CH₄ sample (≈ 1), respectively.

The optical power output from the waveguide is converted to an electric signal $u_r(t)$ by a detector, expressed as

$$u_r(t) = KD_{\text{oe}} P_0(t) [1 + m u_{\text{WMS}}(t)] \exp(-\gamma \alpha_{\text{gas}}(t) CL - \alpha_{\text{int}} L) \quad (7)$$

where m is the light intensity modulation coefficient, and K and D_{oe} are amplifying factor and photoelectric conversion coefficient, respectively.

The schematic diagram in Fig. 1(a) also shows how the second harmonic ($2f$) signal $A_{2f}(t)$ is generated. The $A_{2f}(t)$ extracted from the LabVIEW-based orthogonal lock-in amplifier can be expressed as

$$A_{2f}(t) = \sqrt{(A_{2f,\perp})^2 + (A_{2f,\parallel})^2} \quad (8)$$

where $A_{2f,\perp}$ and $A_{2f,\parallel}$ are the two orthogonal components. The amplitude of the $2f$ signal ($\max(A_{2f})$) is related to C and absorption peak wavelength, which is used for gas concentration calibration.

During a long-term WMS detection of a gas sample with a concentration level of C , define the mean value of the measured $2f$ signal amplitude as $\overline{\max(A_{2f})}$, and the 1σ noise of the measurement result as $n_{1\sigma}$, where σ represents the standard deviation. Then the SNR of the sensor can be calculated by $\overline{\max(A_{2f})} / n_{1\sigma}$. Therefore the LoD of the sensor with a good linear response can be expressed as [19].

$$LoD = \frac{C}{SNR} = \frac{C n_{1\sigma}}{\max(A_{2f})} \quad (9)$$

Here, $n_{1\sigma}$ will be experimentally derived through CH₄ measurement (see Section 4.3).

3. Optimization and simulation of optical waveguide sensor

3.1. Waveguide structure and optimization

Rectangular waveguide [22–24] and suspended waveguide [7,25] are two typical waveguide structures used for gas sensing based on infrared absorption. However, a trapezoid waveguide is easily obtained when fabricating a ChG rectangular waveguide using lift-off technique [19]. The structure of the ChG trapezoid, rectangular and suspended waveguide are shown in Fig. 2(a), (b) and (c), respectively. Compared with ChG-on-SiO₂ waveguide, since the refractive index of MgF₂ is lower

than that of SiO₂, the light power in the under cladding layer is smaller resulting in a higher γ [19]. Besides, compared with SiO₂ with an operating wavelength less than 3.6 μm , the transparency window of MgF₂ can be up to ~ 7 μm , which makes the ChG-on-MgF₂ waveguide operate in a wider wavelength range. Since the laser emitting beam is polarized along the vertical direction, the three waveguide structures with the quasi-TM₀ mode are optimized to increase γ using COMSOL Multiphysics. A similar optimized method can be seen in our previous work [13,14] and the optimized results are shown in Table 1. At 3.291 μm , the calculated γ of the three waveguides are 0.078, 0.151 and 1.152, respectively. The optical mode field distribution are shown in the insets of Fig. 4(a), (b) and (c), respectively. Compared to the trapezoid and rectangular structure, the suspended waveguide with $\gamma = 1.152$ shows enhanced light-gas interaction effect by exposing more mode field to analyte, which is larger than the light-gas interaction in free space ($\gamma = 1.0$).

3.2. Influences of waveguide loss and external confinement factor

Curves of the $2f$ signal amplitude $\max(A_{2f})$ versus the waveguide loss α_{int} is shown in Fig. 3(a), where $\gamma = 0.078, 0.151$ and 1.152 for the three waveguides, $L = 1$ cm and 2 cm, and $C = 1\%$ ($1\% = 10,000$ ppm, parts per million). The $\max(A_{2f})$ decreases with the increase of α_{int} because of the decrease of output light power. So a waveguide with lower α_{int} shows better performances. The total optical loss of the 2 cm-long waveguide increases more obviously than that of the 1 cm-long waveguide with the increase of α_{int} , leading to a smaller output power. So the $\max(A_{2f})$ of the 2cm-long waveguide sensor decreases more obviously with the increase of α_{int} . When α_{int} reaches 5.5 dB/cm, the $\max(A_{2f})$ of the 1 cm-long trapezoid waveguide is close to the noise level $n_{1\sigma}$ (the experimental result in Section 4.3), and at this time, $SNR \approx 1$. When α_{int} increases from 1 dB/cm to 3 dB/cm, the $\max(A_{2f})$ decreases by ~ 2.5 times. Generally, the α_{int} of a reported ChG waveguide can be < 3 dB/cm [26–28], which will be considered in the following simulation.

The simulated $\max(A_{2f})$ versus γ and the linear fitting lines are shown in Fig. 3(b), where $L = 1$ cm and 2 cm, $\alpha_{\text{int}} = 1$ dB/cm and $C = 1\%$. The waveguide with large γ can increase SNR. Typically, the γ of a suspended waveguide can be > 1 but the fabrication process needs two lithography

Table 1

Optimized results of the ChG trapezoid, rectangular and suspended waveguide at 3.291 μm .

Waveguide	Mode	Structural parameters	Value (μm)	γ
Trapezoid	Quasi-TM ₀	Top width, w_1	2.8	0.078
		Bottom width, w_2	6.4	
Rectangular	Quasi-TM ₀	Strip height, h	1	0.151
		Strip width, w_3	3	
Suspended	Quasi-TM ₀	Strip height, h	0.45	1.152
		Strip width, w_3	4	
		Strip height, h	0.1	
		Planar layer width, W	8	
		Planar layer height, H	0.3	

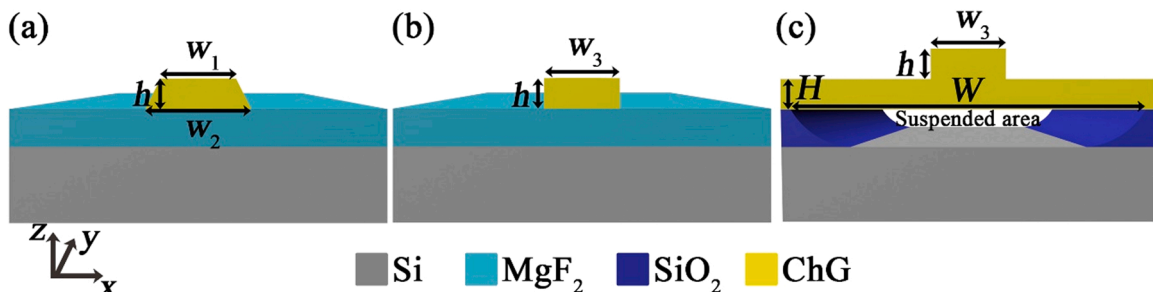


Fig. 2. Structures of (a) trapezoid, (b) rectangular and (c) suspended waveguides.

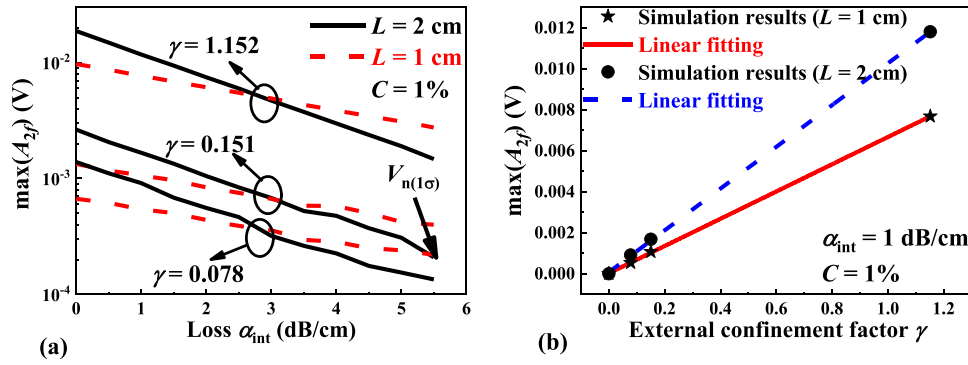


Fig. 3. (a) The simulation curves of the $2f$ signal amplitude $\max(A_{2f})$ versus waveguide loss α_{int} , where $\gamma = 0.078, 0.151$ and 1.152 , $L = 1$ cm and 2 cm, and $C = 1\%$. (b) Curves of the simulated data dots of $\max(A_{2f})$ versus γ as well as the linear fitting curves, where $L = 1$ cm and 2 cm, $\alpha_{\text{int}} = 1$ dB/cm and $C = 1\%$.

steps [7]. The γ of a slot waveguide can be larger than a rectangular waveguide, but the fabrication of the slot waveguide requires high-precision electron beam lithography process and the larger scattering loss caused by dry etching limits the sensing performance [29].

3.3. Influence of waveguide sensor length

Curves of the simulated $\max(A_{2f})$ of the three waveguide modes versus L are shown in Fig. 4(a), (b) and (c), respectively, where $\alpha_{\text{int}} = 0$ dB/cm, 1 dB/cm, 2 dB/cm, and 3 dB/cm and $C = 1\%$. The $\max(A_{2f})$ increases linearly with the increase of L when $\alpha_{\text{int}} = 0$ dB/cm, which can be treated as an ideal condition. When $\alpha_{\text{int}} \neq 0$ dB/cm, the $\max(A_{2f})$ increases first and then decreases as L increases. The waveguide length corresponding to the maximum $\max(A_{2f})$ is defined as the optimal waveguide length L_{opt} . When $L < L_{\text{opt}}$, the increase of L decreases the output power, but the effect of gas absorbance on $\max(A_{2f})$ is larger than that of α_{int} . However, when $L > L_{\text{opt}}$, the effect of α_{int} on $\max(A_{2f})$ is more obvious than that of absorbance. Curves of L_{opt} of the three waveguide

sensors versus α_{int} are shown in Fig. 4(d). L_{opt} decreases with the increase of α_{int} because of the increased waveguide loss. The three waveguides with different γ have the same L_{opt} , indicating that L_{opt} is independent on α_{int} . The $\max(A_{2f})$ becomes larger with the decrease of α_{int} . The simulated curve of $\max(A_{2f})$ for a free-space optical sensor ($\gamma = 1$) is shown in Fig. 4(c), where $C = 1\%$. The $\max(A_{2f})$ of the suspended waveguide sensor with $\alpha_{\text{int}} = 1$ dB/cm is larger than the free-space sensor when $L < 0.6$ cm. However, the $\max(A_{2f})$ of the suspended waveguide with $L < 0.6$ cm is at least 2 times lower than the maximum $\max(A_{2f})$ at $L_{\text{opt}} = 4.3$ cm. This shows that the performance of the suspended waveguide sensor can be better than the free-space sensor with a small L .

For a high precision of performance estimation, a noise level of $n_{1\sigma} = 0.2$ mV is taken in numerical simulation, which was experimentally obtained as can be seen in Section 4.3. Based on Eq. (9), curves of LoD for the three waveguide sensors versus L are shown in Fig. 5(a), (b) and (c), respectively, where $\alpha_{\text{int}} = 1$ dB/cm, 2 dB/cm and 3 dB/cm. The LoD of the suspended waveguide sensor with $\alpha_{\text{int}} = 1$ dB/cm is 145 ppm, which

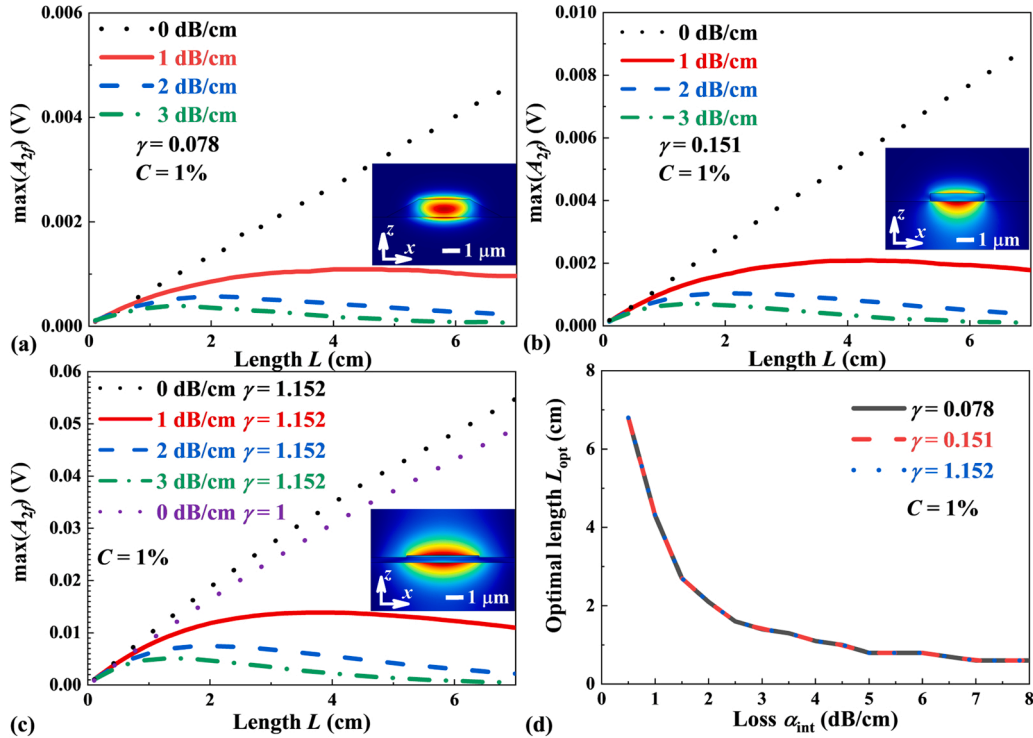


Fig. 4. Curves of the simulated $2f$ signal amplitude $\max(A_{2f})$ of (a) trapezoid, (b) rectangular and (c) suspended waveguides versus L , where $\alpha_{\text{int}} = 0$ dB/cm, 1 dB/cm, 2 dB/cm, and 3 dB/cm and $C = 1\%$. Insets: The optical field distribution of the corresponding waveguides. (d) Curves of the optimal waveguide length L_{opt} versus waveguide loss α_{int} , where $\gamma = 0.078, 0.151$ and 1.152 , and $C = 1\%$.

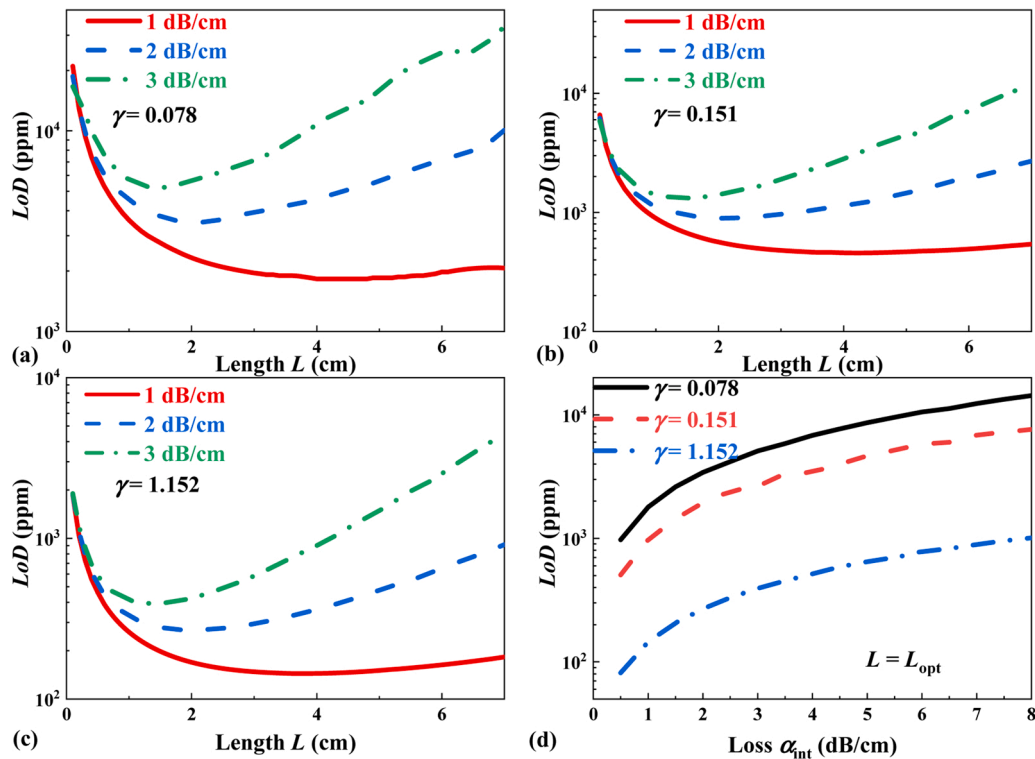


Fig. 5. Curves of LoD for (a) trapezoid, (b) rectangular and (c) suspended waveguides versus L , where $\alpha_{\text{int}} = 1$ dB/cm, 2 dB/cm, and 3 dB/cm and $C = 1\%$. (d) Curves of LoD versus α_{int} , where $\gamma = 0.078, 0.151$ and 1.152 , and $L = L_{\text{opt}}$.

is > 6 times smaller than the LoD of the rectangular waveguide. In the absence of absorption enhancement effect (e.g., slow light effect [15,16,30,31] and surface-enhanced infrared absorption effect [32]), the LoD of a waveguide sensor with small length is difficult to reach a parts-per-billion (ppb) level. According to the linear relationship between γ and $\max(A_{2f})$ in Fig. 4(b) and the rectangular waveguide performances, the LoD of the waveguide with the optimal length can be < 1000 ppm when $\gamma > 0.145$ ($\alpha_{\text{int}} = 1$ dB/cm), 0.290 ($\alpha_{\text{int}} = 2$ dB/cm) and 0.428 ($\alpha_{\text{int}} = 3$ dB/cm). Curves of LoD for the three waveguides versus α_{int} are shown in Fig. 5(d), where $L = L_{\text{opt}}$. As can be seen that either increasing γ , or decreasing α_{int} or choosing appropriate L are effective methods to improve the performances of waveguide sensor. The performances of the three waveguides with optimal length are shown in Table 2.

3.4. Analysis of the optimal waveguide sensor length

Due to the use of wide coupled waveguides on both sides of the sensing waveguide (the trapezoid fabricated waveguide structure in Section 4.1), the sensing waveguide length cannot be changed after fabrication, so it is necessary to select an appropriate waveguide length

Table 2
Simulated performances of the three waveguide sensors with optimal length.

Waveguide	Mode	α_{int} (dB/cm)	L_{opt} (cm)	$\max(A_{2f})$ (V)	LoD (ppm)
Trapezoid	Quasi-TM ₀	1	4.3	0.00110	1790
		2	2.1	0.00060	3407
		3	1.4	0.00040	5093
Rectangular	Quasi-TM ₀	1	4.3	0.00209	957
		2	2.1	0.00104	1923
		3	1.4	0.00070	2837
Suspended	Quasi-TM ₀	1	4.3	0.01379	145
		2	2.1	0.00743	269
		3	1.4	0.00509	393

before fabrication. The simulation results in Fig. 4(d) show that the variation of γ has no influence on L_{opt} . So α_{int} is only considered in optimizing L_{opt} . The α_{int} of the reported ChG waveguide sensors was usually ≤ 8 dB/cm [19,26,28,32], and it is a challenge to fabricate a ChG waveguide with $\alpha_{\text{int}} \leq 1$ dB/cm. Based on Fig. 4(d), the corresponding range of L_{opt} is 2.7–0.6 cm when $1.5 \leq \alpha_{\text{int}} \leq 8$ dB/cm. Under the case of $\alpha_{\text{int}} = 1.5$ dB/cm (i.e. the measured waveguide loss in this work), the $\max(A_{2f})$ of the waveguides with $L = 1$ cm and $L = 2$ cm are 0.703 times and 0.967 times of the waveguide with $L_{\text{opt}} = 2.7$ cm, respectively.

4. Waveguide sensor fabrication and experiment

4.1. Fabrication of ChG-on-MgF₂ waveguide

The fabrication process of the ChG-on-MgF₂ waveguide is shown in Fig. 6. A MgF₂ film was deposited on the silicon (Si) substrate by thermal evaporation (IT-302, LJUHV). MgF₂ has a high transmittance in the MIR with a refractive index of ~ 1.39 . Then a Ge₂₈Sb₁₂Se₆₀ core layer was fabricated on MgF₂ layer by lift-off method [19]. The lift-off method requires different exposure doses at the top and bottom of the photoresist to form an undercut structure after developing. The undercut structure of photoresist can ensure the success of using lift-off method for waveguide fabrication, but a trapezoid waveguide other than a rectangular waveguide is usually formed due to the undercut photoresist structure. The refractive index of Ge₂₈Sb₁₂Se₆₀ is ~ 2.63 at ~ 3.291 μm . CH₄ was adopted as the upper cladding layer with a targeted absorption wavelength of ~ 3.291 μm . Following the optimization results in Section 3.4, the waveguide length was selected as $L = 1$ cm and 2 cm for CH₄ sensing. The schematic diagrams of the straight ChG-on-MgF₂ waveguides (WG1) with a length of $L_1 = 1$ cm and the meander ChG-on-MgF₂ waveguides (WG2) with a length of $L_2 = 2$ cm are shown in Fig. 7(a). The bending radius of WG2 was 50 μm and the bending loss can be ignored. A polydimethylsiloxane (PDMS) gas cell (16 mm \times 10 mm \times 10 mm) with an inlet and an outlet was bonded on the chip. The width of

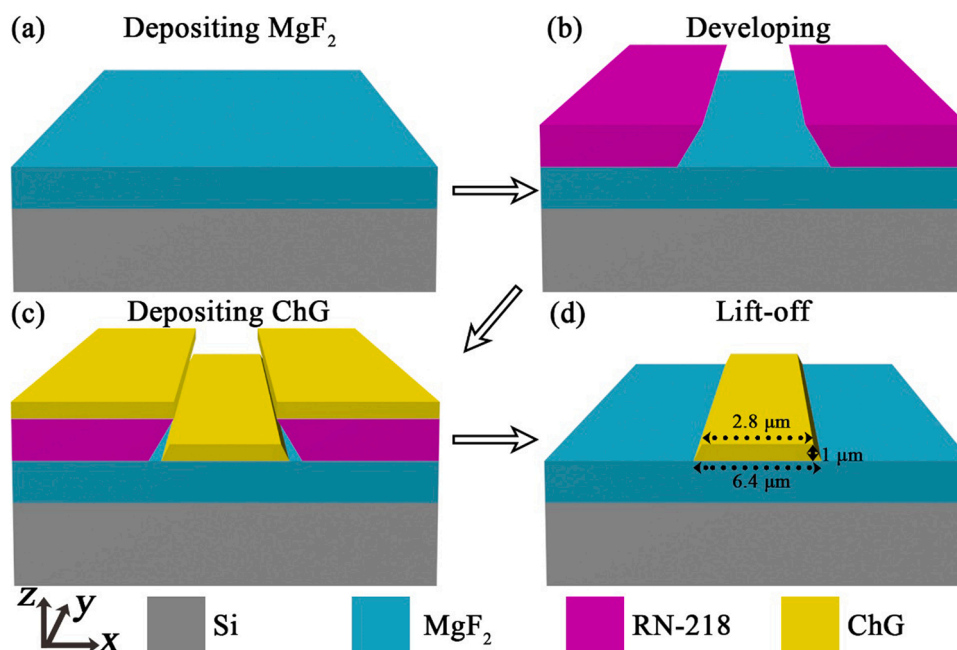


Fig. 6. The fabrication process of the ChG-on-MgF₂ waveguide.

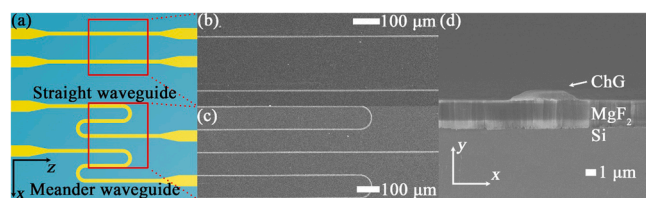


Fig. 7. (a) Top-view structure of the straight and meander waveguides. The SEM images of (b) straight waveguide, (c) meander waveguide, and (d) waveguide cross-section structure.

the coupled waveguides on both sides of the sensing waveguide were increased to 16 μm . The scanning electron microscope (SEM) images of the straight waveguides and meander waveguides are shown in Fig. 7(b) and (c), respectively. The SEM image of the waveguide cross-section structure is shown in Fig. 7(d). The thickness of the MgF₂ lower cladding layer is 2.7 μm and the structural parameters of ChG core layer are the same as those of the trapezoid waveguide in Table 1. The quasi-TM₀ mode optical field distribution is shown in the inset of Fig. 4(a).

4.2. Sensor system

A schematic diagram of the waveguide gas sensor system based on WMS is shown in Fig. 8. The function of the orthogonal lock-in amplifier was realized by a LabVIEW-based lock-in amplifier. The low-pass filter was realized by a second-order Butterworth filter, and the high cutoff frequency and low cutoff frequency were set as 0.45 Hz and 0.125 Hz, respectively. A current driver and a temperature controller were used to drive the ICL (Nanoplus, Germany) with transverse magnetic (TM) polarization and a beam diameter of ~ 4 mm. The light from the ICL with an emission wavelength of ~ 3.291 μm was coupled to a single mode (SM) indium fluoride (InF₃) fiber (Le Verre Fluoré, France) by a reflective collimator (RC08, Thorlabs, USA). The ChG-on-MgF₂ waveguide was butt-coupled with the SM fiber and the output light of the waveguide was detected by a mercury cadmium telluride (MCT) detector (PVI-4TE-5, VIGO System, Poland). The signal output from the detector was derived by a data acquisition (DAQ) card (USB 6361, National Instruments) and processed by a LabVIEW platform to obtain the 2f

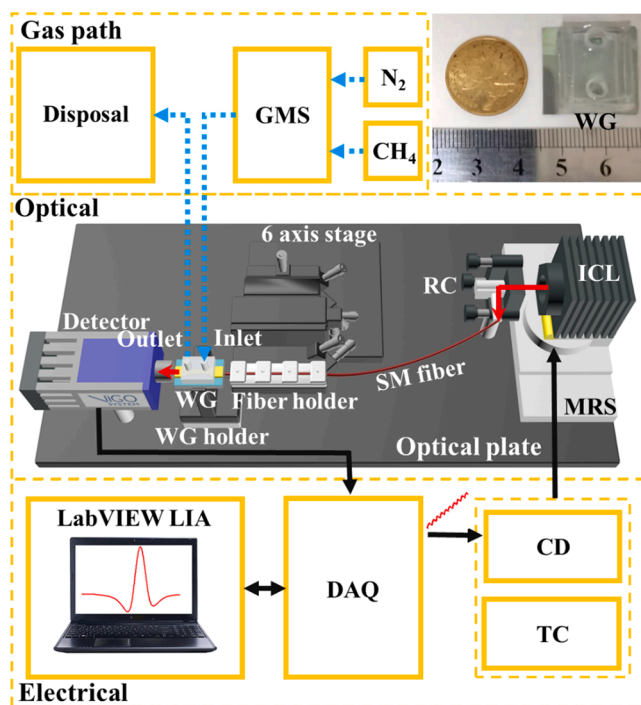


Fig. 8. Schematic diagram of the waveguide gas sensor system based on WMS. WG: waveguide; RC: reflective collimator; SM: single mode; MRS: manual rotation stage; CD: current driver; TC: temperature controller; DAQ: data acquisition; GMS: gas mixing system; LIA: lock-in amplifier. Inset: the sensor chip with PDMS gas cell.

signal. The DAQ card generated a triangular wave signal superimposed by a sine wave signal to the current driver to drive the ICL. A gas mixing system (EnviroNics, Series 4000) controlled the flow rate of CH₄ (99.999%) and nitrogen (N₂) (99.999%) to obtain CH₄ samples with different concentration levels.

4.3. CH₄ sensing results

First, the waveguide loss was determined without modulating the laser. The temperature of the ICL was set to 16 °C. The current range was 45–55 mA and the scan signal frequency was set to 10 Hz to cover the CH₄ absorption line. Since the atmospheric CH₄ concentration level is only ~ 2 ppm [33], the absorption outside the PDMS gas cell can be ignored compared to the absorption in the gas cell with a CH₄ concentration level of 20%. WG1 and WG2 were measured at $C = 20\%$ with a flow rate of 100 sccm. Under the operation of only a triangle wave signal for wavelength scan of the ICL, the measured output signal from the detector and the linear fitting curves for WG1 and WG2 are shown in Fig. 9(a). Under the same input power and coupling method, the waveguide loss can be calculated by the measured voltage of WG1 (Amp_{L2}) and WG2 (Amp_{L1}) as $\alpha_{int} = -10 \log_{10}(Amp_{L2}/Amp_{L1})/(L_2-L_1) = 1.52 \text{ dB/cm}$. The coupling loss from the MIR fiber to the waveguide was measured to be ~ 6.6 dB.

Then the sensing performance of WG1 and WG2 based on WMS were analyzed. A sinewave with a frequency of 5 kHz was added to the previous triangular wave. Curves of $\max(A_{2f})$ and modulation depth versus modulation amplitude are shown in Fig. 9(b), where the CH₄ concentration is 20%. The modulation amplitude was optimized as 0.03 V to obtain the largest $\max(A_{2f})$ and the corresponding modulation depth was 0.08849 cm^{-1} . CH₄ samples with concentration levels of 0%, 10%, 20% and 30% were flowed into the gas cell at a flow rate of 100 sccm. Before injecting CH₄ samples into the gas cell, pure N₂ was passed into the gas cell to remove the residual CH₄. The 2f signals of WG1 and WG2 at different CH₄ concentration levels from 10% to 30% are shown in Fig. 10(a) and (c), respectively. The average value of $\max(A_{2f})$ for WG1 and WG2 at $C = 20\%$ are 2.28 mV and 4.08 mV, respectively. The data dots of $\max(A_{2f})$ at each CH₄ concentration level from 0% to 30%, the corresponding fitting curves for WG1 and WG2 and the simulated $\max(A_{2f})$ data dots are shown in Fig. 10(b) and (d), respectively. The simulation results are consistent with the experimental results, which shows a good accuracy of the simulation model. The fitting equation between CH₄ concentration (in ppm) and the $\max(A_{2f})$ (in V) of WG1 and WG2 are

$$C_{WG1} = 1.5091 \times 10^8 \max(A_{2f}) - 5.9187 \times 10^4 \quad (10)$$

$$C_{WG2} = 7.7124 \times 10^7 \max(A_{2f}) - 1.4675 \times 10^4 \quad (11)$$

where C_{WG1} and C_{WG2} are CH₄ concentration of WG1 sensor and WG2 sensor, respectively.

Pure N₂ was flowed into the PDMS gas cell for analyzing the Allan deviation of the sensor. The measured CH₄ concentration for WG1 and WG2 versus measurement time in N₂ environment are shown in Fig. 11 (a) and (b), respectively. In addition to the temperature drift of the

detector and environmental vibration, other noises include the dilution ratio variation of the gas mixing system, the fluctuation of laser power and mode interference of the waveguide and fiber. The 1σ noise (defined as $n_{1\sigma}$) for WG1 and WG2 are 0.25 mV and 0.15 mV, respectively. Based on Eq. (9), the LoD of WG1 and WG2 were calculated as 2.2% and 0.7%, respectively. The LoD of WG2 based on WMS decreased by > 3 times compared to WG1. The Allan deviation curves of WG1 and WG2 versus averaging time are shown in Fig. 11(c). The data acquisition time (i.e. minimum averaging time) is 0.2 s, which includes the signal sampling time of 0.1 s and the data processing time of 0.1 s. For a linear system, the LoD is usually determined by standard deviation or Allan deviation. With the increase of averaging time, the white Gaussian noise of the sensor is reduced, resulting in the decrease of Allan deviation and a lower LoD. However, as the averaging time increases to a certain value, system drift starts to play a dominant role, leading to the increase of Allan deviation and LoD. The LoD of WG1 and WG2 are 0.68% (6784.2 ppm) and 0.17% (1727.1 ppm) at an averaging time of 0.2 s, respectively, which are in the same order of magnitude as the LoD calculated based on Eq. (9). The LoD of WG2 is 140.8 ppm at an optimum averaging time of 32.4 s and the LoD of WG1 is 396.7 ppm at an optimum averaging time of 81.8 s

5. Comparison and discussion

5.1. Comparison between simulation and experiment

Under the case of $\alpha_{int} = 1.52 \text{ dB/cm}$ and $C = 30\%$, simulated curves of $\max(A_{2f})$ versus L as well as the measured $\max(A_{2f})$ of the two waveguide sensors are shown in Fig. 12. As can be seen, the two measured data dots are on the simulated line, which verifies a good agreement between experiment and simulation. A detailed comparison between the simulation and experiment results are summarized and shown in Table 3, from which a similar conclusion can be drawn. Therefore, the proposed formulation and simulation procedure are effective and accurate in the design of such waveguide sensors prior to fabrication. It should be note that, waveguide loss is quite important in device optimization, which needs to be precisely determined first based on measurement.

5.2. Comparison with other waveguide sensors

A comparison between the MIR ChG waveguide CH₄ sensors is shown in Table 4. Compared with other ChG-on-SiO₂ rectangular waveguides, the proposed ChG-on-MgF₂ waveguides have the smallest α_{int} , which makes a great contribution to the improvement of $\max(A_{2f})$ and SNR. The γ of the proposed waveguide is in the same order of magnitude than other ChG-on-SiO₂ waveguides in Refs. [22,24]. The optical part and gas sampling path part of the proposed sensor system are the same as our

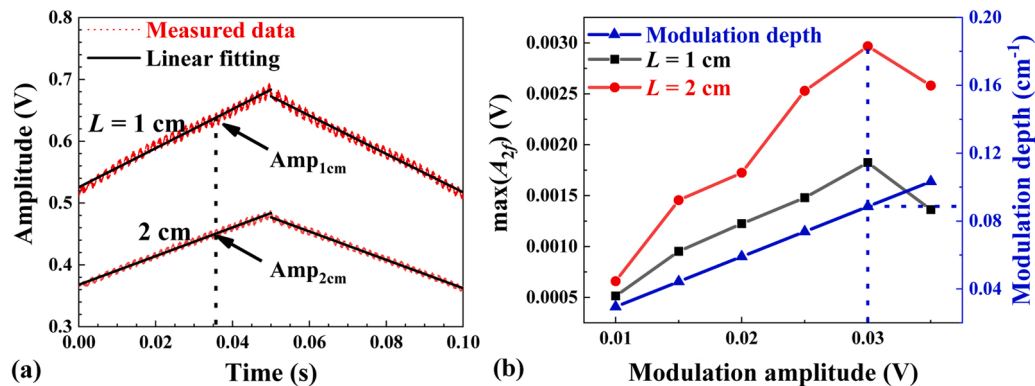


Fig. 9. (a) Under the operation of only a triangle wave signal for wavelength scan, the measured output signal from the detector and the linear fitting curves for WG1 and WG2. (b) Curves of $\max(A_{2f})$ and modulation depth versus modulation amplitude, where the CH₄ concentration level is 20%.

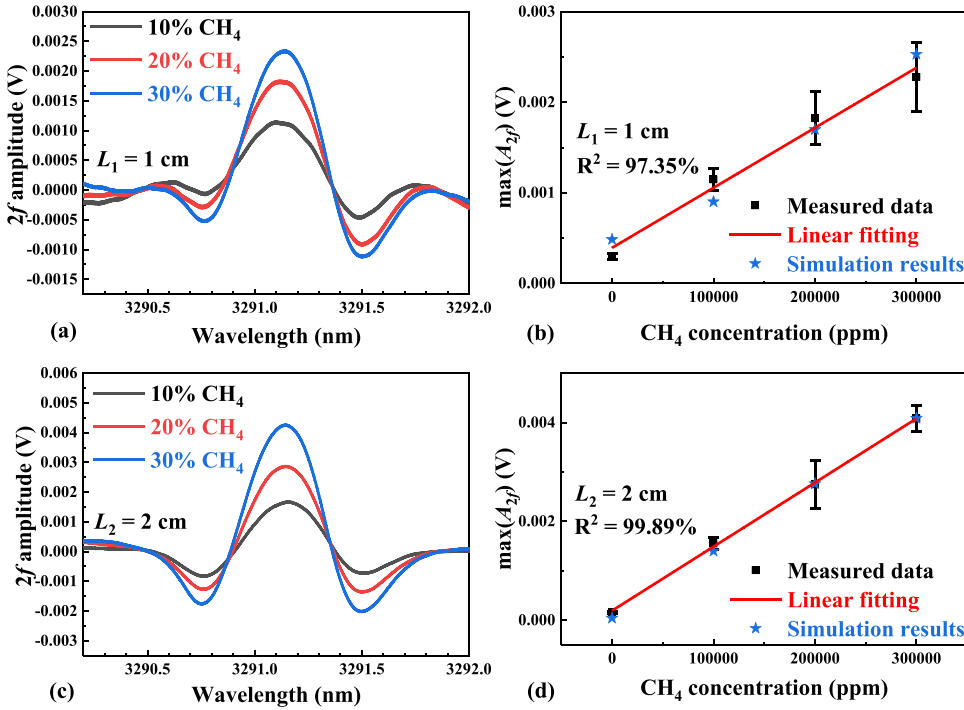


Fig. 10. (a) The measured $2f$ signal of WG1 at different CH_4 concentration levels from 10% to 30%. (b) The measured data dots of $\max(A_{2f})$ at a CH_4 concentration level from 0% to 30%, the corresponding fitting curves of WG1 as well as the simulated data dots of $\max(A_{2f})$. (c) The measured $2f$ signal of WG2 at different CH_4 concentration levels from 10% to 30%. (d) The measured data dots of $\max(A_{2f})$ at a CH_4 concentration level from 0% to 30%, the corresponding fitting curves of WG2 as well as the simulated data dots of $\max(A_{2f})$. R^2 : goodness of fit.

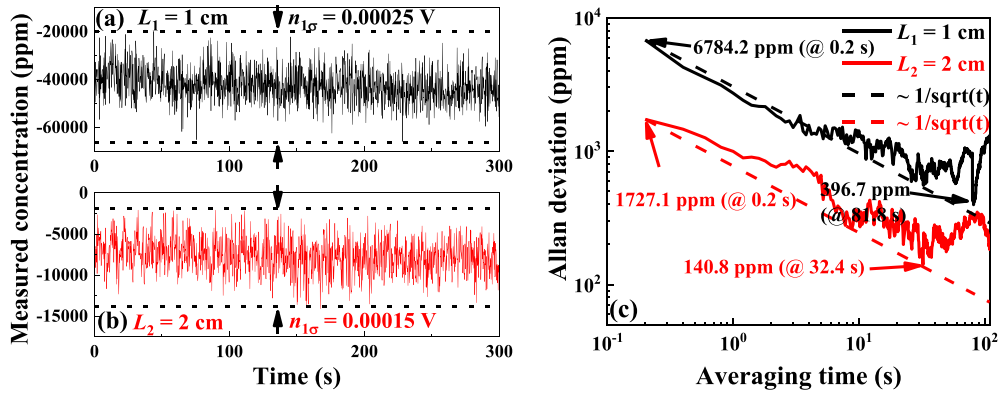


Fig. 11. The measured CH_4 concentration for (a) WG1 and (b) WG2 versus measurement time in N_2 environment. (c) The Allan deviation curves of WG1 and WG2 versus averaging time.

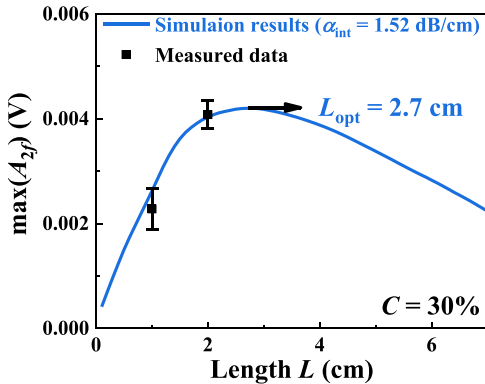


Fig. 12. Simulation curve of $\max(A_{2f})$ versus L and the measured $\max(A_{2f})$ with $L = 1$ cm and $L = 2$ cm, where the CH_4 concentration level is 30% and $\alpha_{\text{int}} = 1.52$ dB/cm.

Table 3

Comparison between the simulation and experimental results for the two waveguide sensors.

Result	Sensor	L (cm)	$\max(A_{2f})$ (mV)	LoD
Simulation	Straight sensor	1	0.00262	2.9%
Experiment	Straight sensor	1	0.00228	2.2%
Simulation	Meander sensor	2	0.00403	1.1%
Experiment	Meander sensor	2	0.00408	0.7%

previous work [32]. Under the condition of the same sensing waveguide length of 2 cm, the γ with the same order of magnitude and the same CH_4 absorption wavelength of 3291 nm, compared with the ChG-on-SiO₂ waveguide CH_4 sensor, the LoD of the ChG-on-MgF₂ waveguide CH_4 sensor is reduced by > 24 times. Compared with other ChG waveguide CH_4 sensors, our waveguide sensors have the lowest LoD. The product of $\text{LoD} \times L$ of the proposed 2 cm-long waveguide is the smallest, which represents the minimum detectable absorbance. This shows that the performance of the on-chip waveguide gas sensor can be significantly improved by using WMS and our optimization methods. In addition to

Table 4

Comparison among the MIR ChG waveguide CH₄ sensors.

Ref.	Platform	λ (μm)	γ (%)	L (cm)	α_{int} (dB/cm)	Technique	LoD	LoD $\times L$ (cm)
[24]	ChG-on-SiO ₂	3.31	12.5	0.5	8	DAS	1%	5.0×10^{-3}
[22]	ChG-on-SiO ₂	3.31	8	2	7	DAS	2.5%	5.0×10^{-3}
[32]	ChG-on-SiO ₂	3.291	0.5	2	3.6	DAS	4.11% (0.2 s)	8.2×10^{-2}
This work	ChG-on-MgF ₂	3.291	7.8	1	1.52	WMS	0.68% (0.2 s)	6.8×10^{-3}
	ChG-on-MgF ₂	3.291	7.8	2	1.52	WMS	0.17% (0.2 s)	3.4×10^{-3}

waveguide, hollow-core fiber can also be used in gas detection as a chamber [34–36]. Miniaturized on-chip gas detection can be realized by integrating a sensing waveguide, a laser and a detector. However, the length of a hollow-core fiber can be as long as several meters which makes the LoD of a fiber-based gas sensor obviously smaller than a waveguide sensor with a length of only several millimeters.

6. Conclusions

Structural parameters of trapezoid, rectangular and suspended waveguides were optimized to increase the external confinement factor through simulation. The influence of waveguide parameters (α_{int} , L and γ) on the $2f$ signal amplitude ($\max(A_{2f})$) were theoretically analyzed. Noise result obtained from experiment was used to numerically evaluate the LoD for improving the accuracy of the simulation. The simulation results provide a guidance for designing such waveguide sensor based on WMS. Two ChG-on-MgF₂ waveguide CH₄ sensors with a sensing length of 1 cm and 2 cm were fabricated to verify the accuracy of the WMS simulation model and design theory. Based on WMS, the experimentally achieved LoD of WG1 and WG2 were 0.68% and 0.17%, respectively. Using WMS and the optimization method, the LoD of the ChG-on-MgF₂ waveguide CH₄ sensor was reduced by > 24 times compared to the ChG-on-SiO₂ waveguide CH₄ sensor based on DAS. This work provides a detailed theory and performance evaluation method for the design of other on-chip waveguide gas sensors based on WMS. Future work is to fabricate ChG suspended waveguide with a large γ and a reduced noise level for sensing performance improvement.

CRedit authorship contribution statement

Mingquan Pi: Conceptualization, Methodology, Investigation, Writing – original draft. **Yijun Huang:** Investigation. **Huan Zhao:** Investigation, Validation. **Zihang Peng:** Investigation, Validation. **Jiaming Lang:** Investigation. **Jialin Ji:** Investigation. **Ling Teng:** Formal analysis. **Fang Song:** Conceptualization, Investigation, Writing – review & editing. **Lei Liang:** Writing – review & editing. **Chuantao Zheng:** Conceptualization, Investigation, Writing – review & editing, Funding acquisition. **Yu Zhang:** Writing – review & editing. **Yiding Wang:** Resources, Funding acquisition. **Frank K. Tittel:** Writing – review & editing, Supervision.

Declaration of Competing Interest

The authors declare that they have no known competing financial interests or personal relationships that could have appeared to influence the work reported in this paper.

Acknowledgments

The authors wish to express their gratitude to the National Natural Science Foundation of China (Nos. 62175087, 61775079, 61627823, 61960206004), Key Science and Technology R&D Program of Jilin Province, China (No. 20200401059GX), Science and Technology Research Project of Department of Education of Jilin Province, China (No. JJKH20211088KJ), Program for JLU Science and Technology Innovative Research Team (JLUSTIRT, 2021TD-39).

References

- [1] C. Zheng, W. Ye, N.P. Sanchez, C. Li, L. Dong, Y. Wang, R.J. Griffin, F.K. Tittel, Development and field deployment of a mid-infrared methane sensor without pressure control using interband cascade laser absorption spectroscopy, *Sens. Actuators B Chem.* 244 (2017) 365–372.
- [2] B. Li, C. Zheng, H. Liu, Q. He, W. Ye, Y. Zhang, J. Pan, Y. Wang, Development and measurement of a near-infrared CH₄ detection system using 1.654 μm wavelength-modulated diode laser and open reflective gas sensing probe, *Sens. Actuators B Chem.* 225 (2016) 188–198.
- [3] M. Dong, C. Zheng, D. Yao, G. Zhong, S. Miao, W. Ye, Y. Wang, F.K. Tittel, Double-range near-infrared acetylene detection using a dual spot-ring Herriott cell (DSR-HC), *Opt. Express* 26 (2018) 12081–12091.
- [4] F. Song, C. Zheng, W. Yan, W. Ye, Y. Wang, F.K. Tittel, Interband cascade laser based mid-infrared methane sensor system using a novel electrical-domain self-adaptive direct laser absorption spectroscopy (SA-DLAS), *Opt. Express* 25 (2017) 31876–31888.
- [5] Z. Liu, C. Zheng, T. Zhang, Y. Li, Q. Ren, C. Chen, W. Ye, Y. Zhang, Y. Wang, F. K. Tittel, Midinfrared sensor system based on tunable laser absorption spectroscopy for dissolved carbon dioxide analysis in the south china sea: system-level integration and deployment, *Anal. Chem.* 92 (2020) 8178–8185.
- [6] C. Li, C. Zheng, L. Dong, W. Ye, F.K. Tittel, Yiding Wang, Ppb-level mid-infrared ethane detection based on three measurement schemes using a 3.34- μm continuous-wave interband cascade laser, *Appl. Phys. B* 122 (2016) 185.
- [7] M. Vlk, A. Datta, S. Alberti, H.D. Yallev, V. Mittal, G.S. Murugan, J. Jägerská, Extraordinary evanescent field confinement waveguide sensor for mid-infrared trace gas spectroscopy, *Light. Sci. Appl.* 10 (2021) 26.
- [8] B. Kumari, R.K. Varshney, B.P. Pal, Design of chip scale silicon rib slot waveguide for sub-ppm detection of N₂O gas at mid-IR band, *Sens. Actuators B Chem.* 255 (2018) 3409–3416.
- [9] A. Gutierrez-Arroyo, E. Baudet, L. Bodiou, J. Lemaitre, I. Hardy, F. Fajjan, B. Bureau, V. Nazabal, J. Charrier, Optical characterization at 7.7 μm of an integrated platform based on chalcogenide waveguides for sensing applications in the mid-infrared, *Opt. Express* 24 (2016) 23109–23117.
- [10] J. Charrier, M.L. Brandily, H. Lhermite, K. Michel, B. Bureau, F. Verger, V. Nazabal, Evanescent wave optical micro-sensor based on chalcogenide glass, *Sens. Actuators B Chem.* 173 (2012) 468–476.
- [11] A. Gutierrez-Arroyo, E. Baudet, L. Bodiou, V. Nazabal, E. Rinnert, K. Michel, B. Bureau, F. Colas, J. Charrier, Theoretical study of an evanescent optical integrated sensor for multipurpose detection of gases and liquids in the Mid-Infrared, *Sens. Actuators B Chem.* 242 (2017) 842–848.
- [12] B. Kumari, A. Barh, R.K. Varshney, B.P. Pal, Silicon-on-nitride slot waveguide: a promising platform as mid-IR trace gas sensor, *Sens. Actuators B Chem.* 236 (2016) 759–764.
- [13] M. Pi, C. Zheng, R. Bi, H. Zhao, L. Liang, Y. Zhang, Y. Wang, F.K. Tittel, Design of a mid-infrared suspended chalcogenide/silica-on-silicon slot waveguide spectroscopic gas sensor with enhanced light-gas interaction effect, *Sens. Actuators B Chem.* 297 (2019), 126732.
- [14] M. Pi, C. Zheng, Z. Peng, H. Zhao, J. Lang, L. Liang, Y. Zhang, F.K. Tittel, Theoretical study of microcavity-enhanced absorption spectroscopy for mid-infrared methane detection using a chalcogenide/silica-on-fluoride horizontal slot waveguide racetrack resonator, *Opt. Express* 28 (2020) 21432–21446.
- [15] A. Gervais, P. Jean, W. Shi, S. LaRochelle, Design of slow-light subwavelength grating waveguides for enhanced on-chip methane sensing by absorption spectroscopy, *IEEE J. Sel. Top. Quantum Electron.* 25 (2019), 5200308.
- [16] G. Xu, J. Wang, Q. Ji, M. Yang, T. Huang, J. Pan, Y. Xie, P.P. Shum, Design and analysis of slow-light Bloch slot waveguides for on-chip gas sensing, *J. Opt. Soc. Am. B* 37 (2020) 257–263.
- [17] R. Zegadi, N. Lorrain, L. Bodiou, M. Guendouz, L. Ziet, J. Charrier, Enhanced mid-infrared gas absorption spectroscopic detection using chalcogenide or porous germanium waveguides, *J. Opt.* 23 (2021), 035102.
- [18] Y. Qiao, J. Tao, J. Qiu, X. Hong, J. Wu, Sensitive and ultrasmall sample volume gas sensor based on a sealed slot waveguide, *Appl. Opt.* 58 (2019) 4708–4713.
- [19] M. Pi, C. Zheng, H. Zhao, Z. Peng, J. Lang, J. Ji, L. Liang, Y. Zhang, Y. Wang, F. K. Tittel, Mid-infrared ChG-on-MgF₂ waveguide gas sensor based on wavelength modulation spectroscopy, *Opt. Lett.* 46 (2021) 4797–4800.
- [20] J.T. Robinson, K. Preston, O. Painter, M. Lipson, First-principle derivation of gain in high-index contrast waveguides, *Opt. Express* 16 (2008) 16659–16669. (<https://hitran.org/>).
- [21] Z. Han, P. Lin, V. Singh, L. Kimerling, J. Hu, K. Richardson, A. Agarwal, D.T.H. Tan, On-chip mid-infrared gas detection using chalcogenide glass waveguide, *Appl. Phys. Lett.* 108 (2016), 141106.

- [23] L. Tombez, E.J. Zhang, J.S. Orcutt, S. Kamapurkar, W.M.J. Green, Methane absorption spectroscopy on a silicon photonic chip, *Optica* 4 (2017) 1322–1325.
- [24] P. Su, Z. Han, D. Kita, P. Becla, H. Lin, S. Deckoff-Jones, K. Richardson, L. C. Kimerling, J. Hu, A. Agarwal, Monolithic on-chip mid-IR methane gas sensor with waveguide-integrated detector, *Appl. Phys. Lett.* 114 (2019), 051103.
- [25] F. Ottonello-Briano, C. Errando-Herranz, H. Rödjegård, H. Martin, H. Sohlström, K. B. Gylfason, Carbon dioxide absorption spectroscopy with a mid-infrared silicon photonic waveguide, *Opt. Lett.* 45 (2020) 109–112.
- [26] X. Gai, S. Madden, D.Y. Choi, D. Bulla, B. Luther-Davies, Dispersion engineered $\text{Ge}_{11.5}\text{As}_{24}\text{Se}_{64.5}$ nanowires with a nonlinear parameter of $136\text{W}^{-1}\text{m}^{-1}$ at 1550nm, *Opt. Express* 18 (2010) 18866–18874.
- [27] J.F. Viens, C. Meneghini, A. Villeneuve, T.V. Galstian, E.J. Knystautas, M. A. Duguay, K.A. Richardson, T. Cardinal, Fabrication and characterization of integrated optical waveguides in sulfide chalcogenide glasses, *J. Light. Technol.* 17 (1999) 1184–1191.
- [28] X. Gai, D.Y. Choi, S. Madden, B. Luther-Davies, Polarization-independent chalcogenide glass nanowires with anomalous dispersion for all-optical processing, *Opt. Express* 20 (2012) 13513–13521.
- [29] D.M. Kita, J. Michon, S.G. Johnson, J. Hu, Are slot and sub-wavelength grating waveguides better than strip waveguides for sensing? *Optica* 5 (2018) 1046–1054.
- [30] K.M. Yoo, J. Midkiff, A. Rostamian, C. Chung, H. Dalir, R.T. Chen, InGaAs membrane waveguide: a promising platform for monolithic integrated mid-infrared optical gas sensor, *ACS Sens.* 5 (2020) 861–869.
- [31] P. Jean, A. Gervais, S. LaRochelle, W. Shi, Slow light in subwavelength grating waveguides, *IEEE J. Sel. Top. Quantum Electron.* 26 (2020), 8200108.
- [32] M. Pi, C. Zheng, J. Ji, H. Zhao, Z. Peng, J. Lang, L. Liang, Y. Zhang, Y. Wang, F. K. Tittel, Surface-enhanced infrared absorption spectroscopic chalcogenide waveguide sensor using a silver island film, *ACS Appl. Mater. Interfaces* 13 (2021) 32555–32563.
- [33] K. Zheng, C. Zheng, H. Zhang, J. Li, Z. Liu, Z. Chang, Y. Zhang, Y. Wang, F.K. Tittel, Near-infrared off-axis integrated cavity output spectroscopic gas sensor for real-time, in situ atmospheric methane monitoring, *IEEE Sens. J.* 21 (2021) 6830–6838.
- [34] K. Chen, Z. Zhao, X. Zhang, X. Zhang, X. Zhu, Y. Shi, Characterization of gas absorption modules based on flexible mid-infrared hollow waveguides, *Sensors* 19 (2019) 1698.
- [35] J. Li, G. Luo, Z. Du, Y. Ma, Hollow waveguide enhanced dimethyl sulfide sensor based on a 3.3 μm interband cascade laser, *Sens. Actuators B Chem.* 255 (2018) 3550–3557.
- [36] J. Li, S. Yang, Z. Du, R. Wang, L. Yuan, H. Wang, Z. Wu, Quantitative analysis of ammonia adsorption in Ag/AgI-coated hollow waveguide by mid-infrared laser absorption spectroscopy, *Opt. Laser Eng.* 121 (2019) 80–86.

Mingquan Pi received his BS degree from the College of Electronic Science and Engineering, Jilin University, PR China, in 2018. He entered the Ph.D course in 2020. Now he majors in Circuit and System, and his research interests include waveguide gas sensor and optical waveguide device.

Yijun Huang received her BS degree from the College of Electronic Science and Engineering, Jilin University, PR China, in 2021. She entered the master course in the same year. Now she majors in Microelectronics and Solid State Electronics, and her research interests include waveguide gas sensor and optical waveguide device.

Huan Zhao received his BS degree from the College of Electronic Science and Engineering, Jilin University, PR China, in 2017. He entered the Ph.D course in 2019. Now he majors in Circuit and System, and his research interests include hybrid integrated laser and optical waveguide device.

Zihang Peng received his BS degree from the College of Electronic Science and Engineering, Jilin University, PR China, in 2019. He entered the Ph.D course in 2021. Now he majors in Circuit and System, and his research interests include photothermal waveguide gas sensor.

Jiaming Lang received his BS degree from the College of Science, Harbin University of Science and Technology, PR China, in 2019. He entered the master course at Jilin University in the same year. Now he majors in Biomedical Engineering, and his research interests include waveguide gas sensor and optical waveguide device.

Jialing Ji received his BS degree from the College of Electronic Science and Engineering, Jilin University, PR China, in 2020. He entered the master course in the same year. Now he majors in Circuit and System, and his research interests include waveguide gas sensor and optical waveguide device.

Ling Teng received her BS degree from the School of Science, Changchun University of Science and Technology, PR China, in 2018. She entered the master course in 2020. Now she majors in Mathematics, and her research interests include probability theory and mathematical statistics.

Fang Song received her BS degree from the College of Electronic and Information Engineering, Changchun University of Science and Technology, PR China, in 2011. She received her MS and Ph.D degree from the College of Electronic Science and Engineering, Jilin University, PR China, in 2014 and 2020, respectively. Her research interests include Gas and bio-medical sensing techniques and applications.

Lei Liang received his Ph.D degree from the College of Electronic Science and Engineering, Jilin University, PR China, in 2014. Currently he is an associate researcher in State Key Laboratory of Luminescence and Applications, Changchun Institute of Optics Fine Mechanics and Physics, Chinese Academy of Sciences. His research interests include optical waveguide device, semiconductor laser, and SOA.

Yu Zhang received his MS degree and Ph.D degree in 2007 and 2010, respectively, from College of Electronic Science and Engineering, Jilin University, PR China. Now he is a professor in the same college. His research interests include quantum dot materials, LEDs and solar cells.

Chuantao Zheng received his MS degree and Ph.D degree in 2007 and 2010, respectively, from the College of Electronic Science and Engineering, Jilin University, PR China. Currently he is a professor at Jilin University, PR China. His research interests include optoelectronic devices and their applications in sensing and optical communications. Dr. Zheng has published more than 180 scientific journal articles in the above technical fields as a first author or corresponding author.

Yiding Wang received his MS degree in Physics in 1991 from Jilin University. Now he is a professor in State Key Laboratory on Integrated Optoelectronics, College of Electronic Science and Engineering, Jilin University, P.R. China. He is active in the fields of gas sensors using infrared techniques and the fabrication of mid-infrared LEDs and LDs.

Frank K. Tittel received his B.S. degree in 1955 and the Ph.D degree in 1959 from Oxford University. Now he is the J. S. Abercrombie Professor in the School of Engineering, Rice University, Houston, TX. Professor Frank Tittel has been involved in many innovative developments in quantum electronics and laser technology since the discovery of the laser in 1960, with applications ranging from laser spectroscopy to environmental monitoring. The most recent designs utilize novel quantum cascade and interband cascade lasers to achieve compact, robust instrumentation that can be deployed for field applications, such as at NASA's Johnson Space Center related to air and water quality issues relevant to the International Space Station, for urban formaldehyde monitoring funded by the Environmental Protection Agency, as well as the National Institute of Health, for non-invasive NO and CO detection in biomedical systems and the National Science Foundation (<http://lasersci.rice.edu/>).